

${}^3\text{He}(\pi^-,n){}^2\text{H}$ and ${}^4\text{He}(\pi^-,n){}^3\text{H}$ at 50–295 MeV

J. Källne

University of Virginia, Charlottesville, Virginia 22901

J. E. Bolger*

*University of Texas, Austin, Texas 78712*M. J. Devereaux[†] and S. L. Verbeck[‡]*New Mexico State University, Las Cruces, New Mexico 88001*

(Received 26 November 1980)

The cross section of $\pi^- + {}^3\text{He} \rightarrow d + n$ and $\pi^- + {}^4\text{He} \rightarrow t + n$ has been measured at energies between $T = 50$ and 295 MeV and angles between $\theta_n \approx 20^\circ$ and 150° covering the momentum transfer range $q \approx 0.4 - 1.0$ GeV/ c . A phenomenological analysis of the data is attempted to identify the characteristic T , θ , and q dependences of the (π, n) reaction dynamics. Most conspicuous is the angular dependence of the ${}^4\text{He}(\pi^-, n){}^3\text{He}$ which mirrors characteristic features of $\pi + \text{He}$ elastic scattering. The T dependence of (π, n) in ${}^3, {}^4\text{He}$ (for $\theta < 70^\circ$) is similar to $\pi + N$ or $\pi + \text{He}$ elastic scattering. The clear dependence of T and θ is indicative of $\pi + N$ (off-shell) scattering in the basic pion-absorption process. The nuclear form factor q dependence is most pronounced for forward angles, and the largely exponential falloff with q is similar to that of analogous nuclear reactions. Comparisons with theoretical calculations show that crucial ingredients are missing in currently used models and general directions of needed refinements are indicated.

NUCLEAR REACTIONS $\pi^- + {}^3\text{He} \rightarrow d + n$ and $\pi^- + {}^4\text{He} \rightarrow t + n$, $T_\pi = 50 - 295$ MeV, $\theta_n = 20^\circ - 150^\circ$; measured $\sigma(\theta_d, T_\pi)$ and $\sigma(\theta_t, T_\pi)$, discussed reaction mechanisms; the energy and nuclear form factor dependence of the reaction dynamics.

I. INTRODUCTION

The study of nuclear pion absorption (π, N) , or the equivalent (p, π) pion production [in the following we refer to both as (π, N) , where N stands for nucleon] has a long history starting with $\pi d \rightarrow pp$. The first experiment on coherent (π, N) to a discrete nuclear state ($pd \rightarrow t\pi$) was done in the late 1950's.¹ Since then a number of such studies have been conducted and during the last decade these have been extended to include (π, N) on target nuclei of $A > 3$ with maintained separation between different discrete final states; for reviews see Ref. 2.

The $A(\pi, N)A - 1$ reactions in the light nuclei $A \geq 3$ are of particular interest in attempts to find appropriate models to describe the pion-nucleus dynamics characterized by the large momentum mismatch between the incident pion of low momentum and the outgoing nucleon of high

momentum. The effective momentum transfer, defined by $q = |(1 - 1/A)\vec{p}_\pi - \vec{p}_N|$ in the c.m. frame, tells us how much momentum must be absorbed by nuclear dynamics. The large momentum transfer is not *per se* a unique feature of (π, N) , but what distinguishes (π, N) from, for instance, pion or nucleon scattering is the finite minimum value of q defined by the colinear momenta, viz., $(1 - 1/A)p_\pi - p_N \gtrsim 0.4$ GeV/ c . A single nucleon could provide the needed momentum but the probability for finding such a large nuclear (off-shell) momentum is usually vanishingly small. Therefore, a more likely situation is momentum sharing, where, for instance, the pion propagates through the nucleus collecting momentum by successive nucleon interactions before it is absorbed on the nucleon to be ejected. A key element in the latter case is that the pion interaction can take place off the energy shell so that the full momentum transfer

of the reaction is accomplished through incremental increases in the pion momentum by which process each nucleon absorbs its share of the momentum transfer.³

It is not well known how the pion propagates; for instance, how many $\pi + N$ off-shell scatterings are involved and if the nuclear πN interaction should be extended to explicitly invoke other nucleon or meson degrees of freedom^{4–6} such as Δ , ρ , etc., and the subsequent interactions of these particles with the nuclear nucleons. The most specific information on this comes from $\pi d \rightarrow pp$ studies^{3,6–8} which show that both nucleons are part of the absorption process described, for instance,⁸ as $\pi + N_1$ off-shell scattering preceding the $\pi N_2 \rightarrow N_2$ absorption. The $\pi d \rightarrow pp$ reaction provides a starting point in trying to understand $A(\pi, N)A - 1$, $A > 2$. The primary absorption process, however, is then no longer limited to two nucleons, but various reaction mechanisms of different πN multiplicity must be considered and to each mechanism belongs a nuclear form factor (instead of a nucleon form factor for $\pi d \rightarrow pp$) that specifies how the momentum transfer is absorbed by the bound residual nucleus. If the two-nucleon interaction is an important absorption mechanism for $A > 2$, it remains to consider NN states other than the deuteron and their effect on the (π, N) reaction. Interpretational advantages are presented by a small number of nucleons in identical states, as offered by ${}^3\text{He}$ and ${}^4\text{He}$, and detailed reaction models have been worked out for (π, N) reactions in these target nuclei, drawing upon the information available for $\pi d \rightarrow pp$.^{9,10} Another connection between pion absorption in ${}^2\text{H}$ and ${}^3,4\text{He}$ is pion absorption on quasifree NN pairs, $\pi^+ NN \rightarrow Np$, which is a distinct feature¹¹ of the proton spectra ${}^3,4\text{He}(\pi^+, p)X$. The target nuclei ${}^3,4\text{He}$ present favorable conditions to study nuclear pion absorption and the results obtained should be applicable to (π, N) in heavier nuclei with allowance made for effects related to a distinguishable nuclear surface of these target nuclei and to relative nucleon states with $L \neq 0$. Although previous measurements have been reported for ${}^3,4\text{He}$, no comprehensive study has been undertaken. Because of the role that the (π, N) reaction in ${}^3\text{He}$ and ${}^4\text{He}$ plays for advancing our understanding of nuclear (π, N) reactions and other related nucleon reactions, we felt motivated to perform a study of the reactions $\pi^- + {}^3\text{He} \rightarrow d + n$ and $\pi^- + {}^4\text{He} \rightarrow t + n$.

II. EXPERIMENTAL

This experiment was performed with the pion beam of the energy pion channel and spectrometer

system (EPICS) of LAMPF with the aim to measure the pion absorption reactions $\pi^- + {}^3\text{He} \rightarrow n + d$ and $\pi^- + {}^4\text{He} \rightarrow n + t$ by detecting the recoil deuterons and tritons of the (π^-, n) reactions under study. The experiment was run before the magnetic spectrometer was in operation and partly during its installation. In its place we used a detector which had to be compatible with the ongoing construction work; other design considerations were the limited beam time, small reaction cross sections, and the need for a large dynamic detector range. A cryostat,¹² with liquid ${}^3\text{He}$ and ${}^4\text{He}$ targets, was positioned on the ordinary EPICS pivot point. The data acquisition and processing systems were early versions¹³ of those currently used for the complete EPICS channel and spectrometer system. Below we shall describe parts of the equipment and steps in the procedure in some detail.

A. The pion beam

Much of the beam property information needed for this experiment was obtained in special beam measurements before and after our experiment. These include beam phase space, composition, and intensity for which we refer to the special reports available¹⁴ and concentrate here on the particulars of this experiment.

The intensity of the pion beam was limited by the primary proton beam (about 150 μA at the time) and the maximum vertical beam size set by the helium target (10 cm corresponding to the 1% momentum bite of the channel); horizontally, the beam was of standard width, 6.3 cm. For the energy range used, $T = 50 - 295$ MeV, the intensity was $(0.3 - 3) \times 10^6 \pi^-/\text{s}$ which could be decreased as needed with the momentum defining slits in the channel. Two ion chambers (IC) placed 4 m downstream from the pivot recorded the integrated current of π 's and extraneous μ 's and e 's in the beam; protons in the π^+ beam could enter the IC1 but were stopped before reaching IC2 by an aluminium degrader. The pion current incident on the target was deduced from the IC charge on the basis of the relative specific energy losses and the beam composition of π 's, μ 's, and e 's for a given beam momentum. With the help of the measured beam composition for $T = 70 - 295$ MeV we could thus determine the relationship between IC current and pion current IC_π as a smooth IC response function $\kappa(T) = \text{IC}_\pi/\text{IC}$ for $T = 50 - 295$ MeV; the 50 MeV point was obtained by extrapolation. It was normalized to 1 at $T = 200$ MeV for the sake of

convenience. In order to check the response function we measured counts/IC for $\pi^- + p$ scattering from a CH_2 target for elected scattering angles.

With known $\pi^- + p$ cross sections taken from the literature¹⁵ we could make an independent determination of κ , viz.,

$$\kappa \propto \text{IC}_\pi / \text{IC} = (\text{counts}) / \text{IC} [d\sigma/d\Omega(\pi + p)]^{-1}$$

at a few incident energies between 90–295 MeV. The two results for $\kappa(T)$ are shown in Fig. 1. Since the deviation between the individual points and the smooth function $\kappa(T)$ is not statistically significant, we decided to use the smooth curve.

B. Targets

The cryostat¹² used in this experiment was operated at a superfluid temperature ($\approx 1.3^\circ\text{K}$) which was monitored through the measured evaporation pressures of ^3He and ^4He . It held two target cells ($0.64 \times 12.6 \times 12.6 \text{ cm}^3$) containing ^3He and ^4He of the thicknesses 51 and 93 mg/cm^2 , respectively. Extraneous material presented to the incident and outgoing particles in the form of vacuum windows and heat shields amounted to 100 mg/cm^2 Al of which 50 mg/cm^2 was in the external windows at a radius of 36 cm. The target cell assembly was verti-

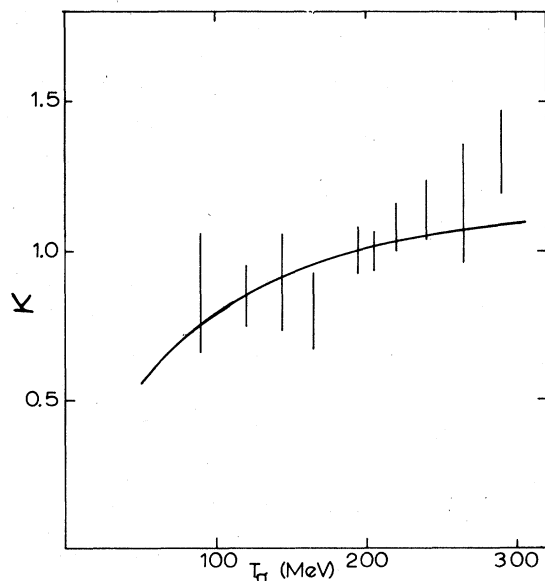


FIG. 1. The ion chamber response function (solid line) compared to the yield of $\pi^- + p$ scattering divided by the known (Ref. 15) cross sections (see the text).

cally movable inside the vacuum vessel for easy target selection. The cryostat was positioned over the pivot and could be rotated on its support table to change the target angle; the target angle was chosen to be perpendicular to the exit particles but limited to $\theta_t \leq 50^\circ$. The table was mounted on rails to allow the cryostat to be moved out of the beam.

The target densities (mg/cm^2) given above were based on the known volume densities of ^3He and ^4He at a given temperature and the nominal target thickness of 0.64 c.m. Considering the temperature contraction and the bulging characteristic of the target cell windows at room temperature, we estimated that the windows ought to be flat at 1.3°K and 40 Torr. An attempt was made to confirm this conclusion by measuring the $\pi^+ + ^4\text{He}$ elastic scattering cross section (using $\pi + p$ scattering as described below) and comparing to published values for $\pi^+ + ^4\text{He}$ at 51 MeV.¹⁶ This indicated, within the uncertainties of $\pm 25\%$, a target thickness consistent with the nominal one.

C. The detector

The detector consisted of three plastic scintillators ($S1$, $S2$, and $S3$) measuring $0.22 \times 13.0 \times 30.2$, $0.32 \times 17.8 \times 59.7$, and $15.2 \times 15.2 \times 50.8 \text{ cm}^3$, with an X - Y wire chamber (WC) placed just in front of $S1$ at a distance of 35 cm from the target (see Fig. 2). $S3$, at the distance of 73 cm, set the limits of the detector acceptance, with the solid an-

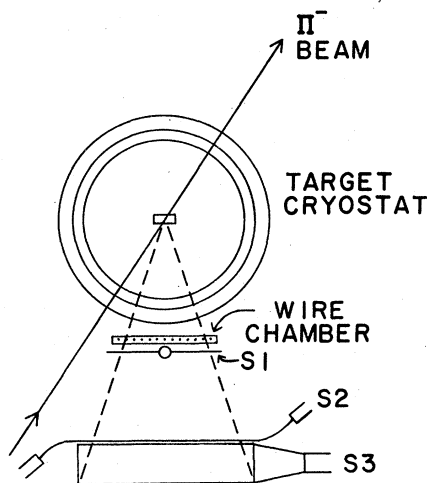


FIG. 2. Schematic top view of cryostat and detector details.

gle being defined by a collimator before $S2$ just in front of $S3$. The total solid angle was 100 msr with 35° angular acceptance in the reaction plane.

To minimize the amount of inactive material in the detector, it was assembled in a light tight box with thin reflecting foils ($13\ \mu\text{m}$ Al) around the scintillators and a thin entrance window before the WC. Particles coming from the far side of the target had to penetrate the equivalent of $420\ \text{mg}/\text{cm}^2$ of $(\text{CH})_n$ to reach $S2$; i.e., the low energy cutoff of the detector was 20, 28, and 33 MeV for protons, deuterons, and tritons. The maximum stopping ranges were $T_p = 148$, $T_d = 200$, and $T_t = 240$ MeV. Photomultiplier tubes (5.1 cm diameter) were looking at two sides of the $S1$ (up and down) and $S2$ (left and right) scintillators, and one 12.7 cm tube was at the right hand side of $S3$ (cf. Fig. 2). The time and pulse height information from these were processed by time-to-digital converters (TDC) and analog-to-digital converters (ADC), while the WC signals were ready by TDC's only. Further data processing was done with a PDP 11/45 computer before storing the data on tape.

The WC provided position information ($X0$ - $Y0$) which was used to apply corrections for the position dependent response of the very thin $S1$ counter. Lateral position information at another point of the particle trajectory ($X2$) was provided by the time difference between the two $S2$ signals, $T(S2_1) - T(S2_2)$; the $X2$ resolution was about 3 cm (FWHM). This information was used to make position dependent response corrections for $S2$ and $S3$. The combined use of $X0$ and $X2$ allowed the determination of the trajectory angle which was used to correct for changes in scintillator thickness seen by particles at nonperpendicular angles and for a change in flight path between $S1$ and $S2$ of importance for the time of flight (TOF) measurement. We also used the $X2$ information to determine the angle of the reaction products from the target relative to the center of the detector.

The detector could be rotated around the pivot and normal angle settings where $\theta_D = 38^\circ, 70^\circ, -100^\circ, -120^\circ, \text{ and } 135^\circ$ (minus signs indicate positions to the right of the beam direction). Each setting covered about 35° and the detector acceptance was subdivided into ten equal slots with the limits defined by $X2$. A few measurements were made with the detector moved out from the pivot, which allowed us to reach more forward angles.

Particle TOF was obtained from the difference between the summed times $T(S1_1) + (TS1_2)$ and $T(S2_1) + T(S2_2)$. This quantity is independent of

position and correcting for change in trajectory angle relative to the scintillator plane was sufficient to eliminate all geometrical effects from affecting the resolution.

There is a similar advantage in using the pulse height products $P(S1) = [P(S1_1)P(S1_2)]^{1/2}$ and $P(S2) = [(P(S2_1)P(S2_2))]^{1/2}$ to determine particle energy losses (ΔE) in the thin counters $S1$ and $S2$. This eliminates most of the distance dependent response variation¹⁷ so that the total geometrical response variation, including effects due to counter nonuniformities, is less than 25% in $P(S1)$ and $P(S2)$. The analysis of the data included corrections for such effects in $S1$ and $S2$, as well as in $S3$, using measured response matrices. These corrections were necessary in order not to degrade the TOF, ΔE , and E resolution beyond the limits set by the photon statistics of the signals. The two-side light collection for the thin scintillators was crucial for obtaining the resolution needed for identifying and separating protons, deuterons, and tritons over a large dynamical range.

To check the performance characteristics and determine response maps, the individual counters were tested with a 3-MeV ${}^{106}\text{Ru}$ electron source. The assembled detector was tested and calibrated in the EPICS beam of π 's, p 's, d 's, and t 's with well defined momentum in the range up to 415 MeV/ c . This made it easy to tune the experiment and it was particularly useful to determine time zero needed to determine TOF, and to match the signals $P(S1)$, $P(S2)$, and $P(S3)$ needed to obtain differential energy losses $\Delta E1$ which could be combined to $E = \Delta E1 + \Delta E2 + \Delta E3$, representing the particle energy. As an illustration of the detector performance we mention that with 415 MeV/ c deuterons we obtained a time resolution of 250 ps with pulse height resolutions (FWHM) of 15% and 8% in $\Delta E1$ and $\Delta E2$, respectively.

For particles of high energy and, hence, large range, nuclear reaction losses in the scintillators become a concern. Such information is not available for d 's and t 's so we made estimates based on the reliable range losses determined for protons¹⁸ and the estimated value for 216-MeV tritons. We assumed that the range losses are of the same functional form $L_A(R) = [L_p(R)]^x$ for p , d , and t , where $L_p(R)$ is the range loss function for protons with the parameter x determined by the $L_{A=3}$ value of Ref. 19 for 216-MeV tritons; $L_{A=2}$ for deuterons was fixed by assuming $x = A$. We also considered the particles close to the top and bottom edges of $S3$ that could escape before stopping. This effect was approxi-

mately 1.5% for $R = 5$ cm and 9% at $R = 15$ cm. Including both this effect and the one due to nuclear reaction losses, we determined the range dependent detector efficiencies shown in Fig. 3.

D. Data acquisition and processing

The time and pulse-height information from the detector was digitized by TDC and ADC and then read into the PDP 11/45 computer for further processing. All events processed by the computer were written to tape and some were subject to reduction and computations on line using an analysis program on a time available basis. An event was defined as a coincidence between the S 1 and S 2 counters, which constituted the main trigger for all electronics.

The computer set the rate at which events could be accepted, but due to the LAMPF beam structure, the macro pulse frequency, 120 Hz, defined the practical rate for 100% acceptance. The number of events rejected by the computer because of busy status was recorded; the rejection rate was small except for the most forward detector setting, where it could reach the 50% level. This was the only dead time correction of any significance since the detector singles rates were always very small compared to the total length of the trigger active

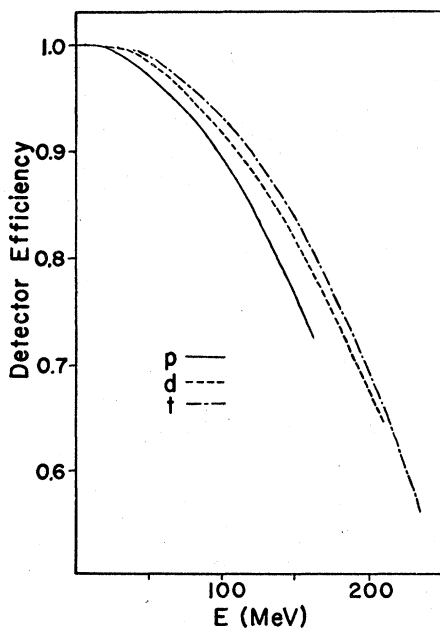


FIG. 3. The detector efficiency as a function of particle energy.

time (~ 250 ns).

The data could be manipulated in one- and two-dimensional displays, for instance, and calculations performed with an analysis program during the experiment to monitor the performance of the experiment. The final data reduction, however, was done afterwards by replaying the tapes. The main objectives of this task were to identify each event by kind of particle and to obtain an energy spectrum where we could unambiguously identify the two-body reactions in the form of a peak.

The particle identification was accomplished in two ways using combinations of E and ΔE , and E and TOF which were proportional to the mass of the particles; i.e., we used functions of the form $E \Delta E^a$ and $E \text{TOF}^b$, where the parameters a and b were adjusted to make the product a constant. The identification was unique since particles of multiple charge were practically all ranged out. Examples of such mass spectra $M(E, \text{TOF})$ and $M(E, \Delta E)$ are shown in Figs. 4 and 5 with four peaks due to π 's, p 's, d 's, and t 's. We also show in the b , c , and d sections of Fig. 5 what the $M(E, \Delta E)$ spectrum looks like when gated on p , d , and t from the $M(E, \text{TOF})$ spectrum. This demonstrates the degree of redundancy available in the particle identification and that clean separation between p , d , t , and other particles was always achieved.

Energy spectra were formed in two ways depending on the range of the particles of interest. If the range was less than 0.7 g/cm^2 , TOF gave the best energy resolution, and for larger ranges E was the preferred variable. Examples of such energy spectra

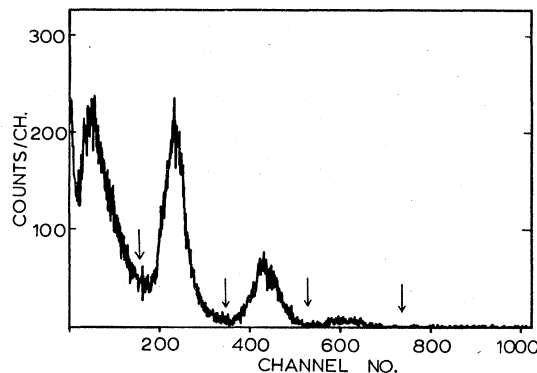


FIG. 4. An example of mass spectrum $M(E, \text{TOF})$ based on measured pulse height for total energy and time of flight (see the text).

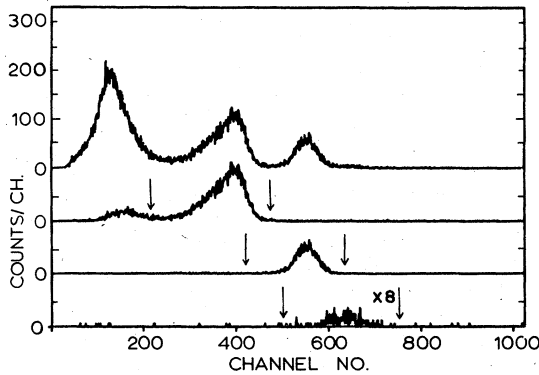


FIG. 5. Examples of mass spectra $M(E, \Delta E)$ based on measured pulse height relating to total and differential energy loss for all particles (a), and for particles identified as protons (b), deuterons (c), or tritons (d) by means of $M(E, \text{TOF})$.

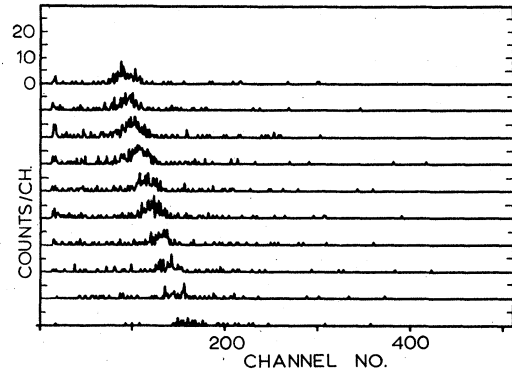


FIG. 7. Example of triton energy spectra based on measured TOF for $T_{\pi^-} = 200$ MeV and $\theta_d = 100^\circ$ with the ${}^4\text{He}$ target. Each spectrum is for an angular acceptance of 3.5° with θ_i running from 86° to 114° (bottom to top spectrum).

are shown in Figs. 6 and 7 for the reactions $\pi^- + {}^3\text{He} \rightarrow d + X$ and $\pi^- + {}^4\text{He} \rightarrow t + X$ for 200 MeV incident pions with the detector set at $\theta_D = 120^\circ$ and 100° , respectively; the abscissas are E and $[1/\text{TOF}]^2$, respectively. Each spectrum corresponds to $\frac{1}{10}$ of the total detector acceptance with the particle angle decreasing from the top to the bottom spectrum as displayed in Figs. 6 and 7. A peak appears in each spectrum corresponding to the $A(\pi^-, n)A - 1$ reaction and the peak position is seen to move with angle in accordance with the (π^-, n) two-body kinematics. The number of

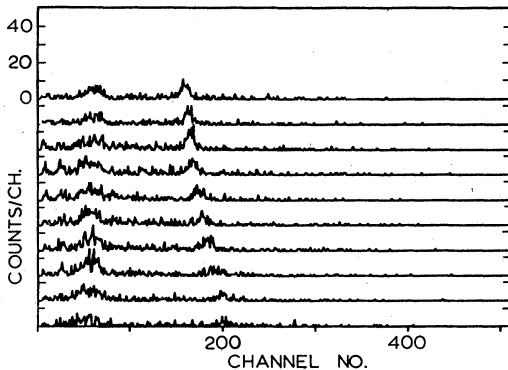


FIG. 6. Example of deuteron energy spectra based on measured pulse height for $T_{\pi^-} = 200$ MeV and $\theta_D = 120^\circ$ with the ${}^3\text{He}$ target. Each spectrum is for an angular acceptance of 3.5° with θ_d running from 106° to 134° (bottom to top spectrum). The bump at around channel 50 is an artifact.

(π^-, n) events were evaluated from these spectra by subtracting a flat background below the peak area where the background level was determined from the counts on both sides of the peak. The spectra were always found to be smooth apart from the (π, n) peak; auxiliary information was always available from the triton/deuteron spectra for ${}^3\text{He}/{}^4\text{He}$, which showed that the background was flat under the triton/deuteron (π^-, n) peak for ${}^4\text{He}/{}^3\text{He}$.

E. Determination of (π^-, n) cross sections

The raw data consisted of the number of counts in the (π^-, n) peak of the spectra described above. This number was corrected for computer dead time and detector efficiency. It was then divided by IC_{π^-} to obtain the (π^-, n) yield per accumulated pion beam charge (in arbitrary units) incident on the target. To collect enough statistics, the yield for a certain pion energy and particle angle was determined from several runs, some of which were distributed over the course of the experiment to check the constancy of the data with time.

Conversion from yield (Y) to cross section ($d\sigma/d\Omega$) was obtained by means of known values¹⁵ for the $\pi^- + p$ scattering cross section at 200 MeV. The $\pi^- + p$ yield was measured for a CH_2 target of well known thickness detecting the proton under conditions identical to those of the recoils from (π^-, n) ; the $\pi^- + p$ scattering formed a distinguishable peak on the smooth background from reactions in ${}^{12}\text{C}$. The differential cross sections of $\pi^- + {}^3\text{He} \rightarrow d + n$ and $\pi^- + {}^4\text{He} \rightarrow t + n$ were thus determined as

$$\frac{d\sigma}{d\Omega}(\pi^-,n) = \frac{Y(\pi^-,n)}{Y(\pi^-+p)} \frac{t(\text{CH}_2)}{t(\text{He})} \frac{d\sigma}{d\Omega}(\pi^-+p),$$

with t expressing the target thickness in number of reaction centers per cm^2 . The uncertainty in the overall normalization is believed to be $\pm 15\%$ at 200 MeV; the *relative* uncertainty over the energy range $T = 100\text{--}295$ MeV is estimated to be $\leq \pm 15\%$ and $\pm 30\%$ for the two lowest energy points. The (π^-,n) differential cross section was determined using an angular bin size of 3.5° for the detected particle. Data points of smaller angle separation, from two different detector settings, for instance, were combined. When poor statistics were the limiting factor to see details in the angular distribution, rather than bin size, a further binning was done; this was not done for the results presented previously.²⁰ All cross sections we present are given in the c.m. frame and the angle is always that of the neutron.

III. RESULTS

In this section we shall present the results by pointing out the salient features of the data. Where previous experiments contribute information complementary to ours, these data are shown as well. Experiments with overlapping data are discussed at the end of this section to sort out corroborating or conflicting measurements.

Our results on differential cross sections of ${}^3\text{He}(\pi^-,n){}^2\text{H}$ and ${}^4\text{He}(\pi^-,n){}^3\text{H}$ are shown in Figs. 8 and 9. The angular distributions for ${}^4\text{He}$ are the ones that display the most pronounced systematic features. They are characterized by a forward angle rise and a more level behavior beyond $\theta \approx 70^\circ$. A second maximum appears at around 90° , always preceded by a clear minimum at a smaller angle. This minimum appears at around 70° and it is also possible to discern a second minimum at 125° in the angular distributions for $T \geq 100$ MeV. In all, these data display oscillations in the (π^-,n) cross section as a function of angle whose maximum/minimum pattern stays remarkably fixed through the energies.

Similar general trends can be seen in the angular distributions of ${}^3\text{He}$ with a steep forward angle slope which changes into a more level behavior in the region of $\theta_n = 60^\circ\text{--}80^\circ$. The lack of oscillations in the ${}^3\text{He}(\pi^-,n){}^2\text{H}$ cross section for $\theta_n > 70^\circ$ and the difference in relative magnitude of the small and large angle (π^-,n) cross sections for ${}^3\text{He}$ and ${}^4\text{He}$ (cf. Fig. 11) are two features that indicate differences

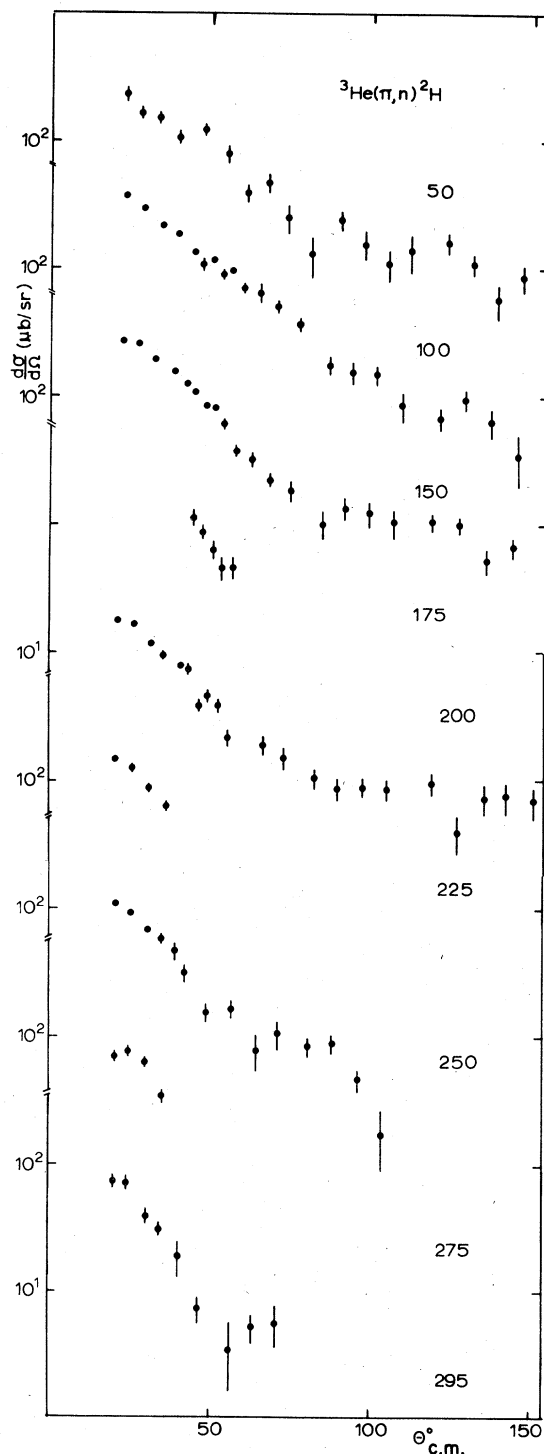


FIG. 8. Results on differential cross sections of $\pi^- + {}^3\text{He} \rightarrow n + {}^2\text{H}$ at energies between 50–295 MeV plotted versus the neutron c.m. angle.

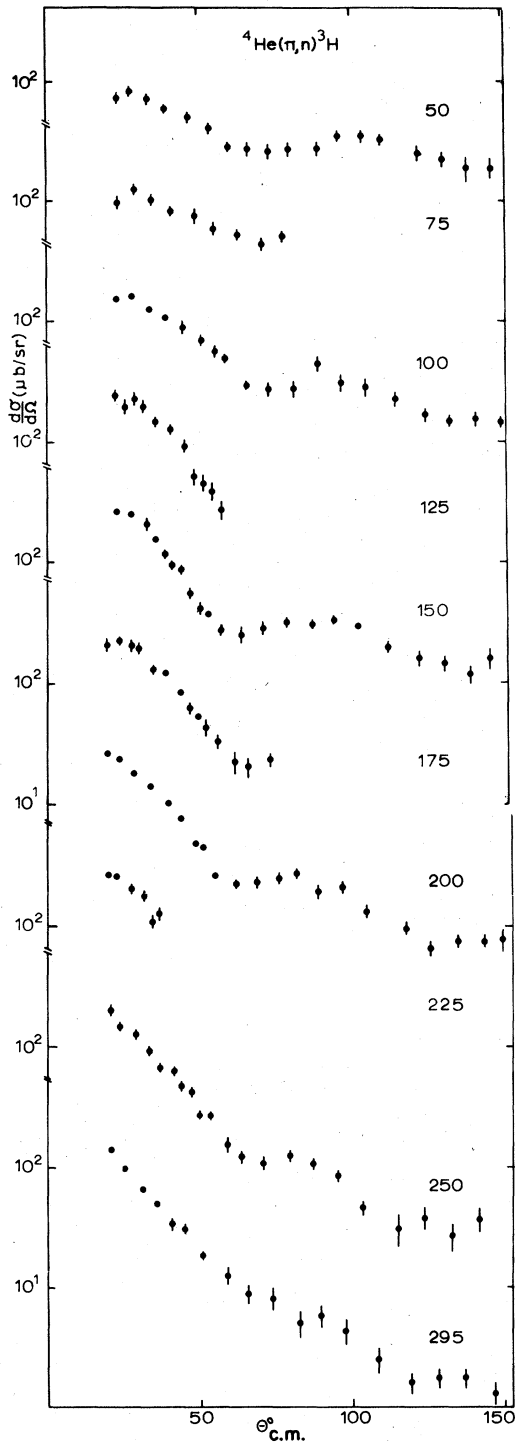


FIG. 9. Results on differential cross sections of $\pi^- + {}^4\text{He} \rightarrow n + t$ at energies between 50–295 MeV plotted versus the neutron c.m. angle.

between these target nuclei to which the (π, n) reaction is sensitive.

The energy dependence of the differential cross section at a fixed angle is shown in Fig. 10. Two points in the angular distributions were chosen as representative of the forward angle cross section and the region around the second maximum of the ${}^4\text{He}$ angular distribution. Characteristic of the small angle (π^-, n) cross section for both ${}^3\text{He}$ and ${}^4\text{He}$ is a pronounced maximum, but they are clearly at different positions, i.e., $T \approx 110$ and 150 MeV, respectively. In comparison the large angle cross section is seen to peak at a smaller energy for both ${}^3\text{He}$ and ${}^4\text{He}$ and the falloff with increasing energy is noticeably slower/faster for ${}^3\text{He}/{}^4\text{He}$ than for the small angle cross section. It thus seems that the resonance behavior of the elementary $\pi + N$ scattering is a principal part of the (π, n) energy dependence, but its full impact is masked by other dynamical factors, some of which are particular to the target and/or residual nuclei in the reaction.

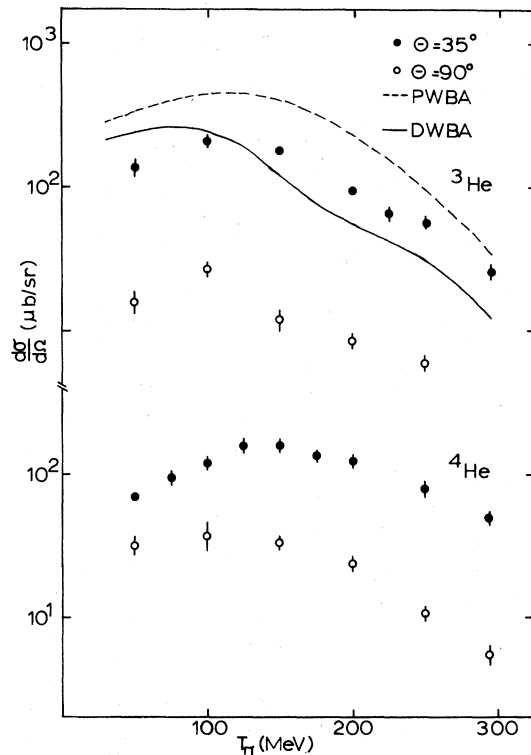


FIG. 10. The differential cross section of ${}^3\text{H}(\pi^-, n){}^2\text{H}$ and ${}^4\text{He}(\pi^-, n){}^3\text{H}$ at $\theta = 35^\circ$ and $90^\circ - 100^\circ$ plotted versus incident pion energy. Predictions (Ref. 10) based on the quasideuteron model with and without distortions are also shown as continuous and dashed curves.

The results on total (π^-, n) cross sections in ^3He and ^4He are shown in Fig. 11 as a function of incident energy. We determined these by angular integration of $d\sigma/d\Omega(\cos\theta)$ with the help of some extrapolation to include unmeasured regions. The error bars include the statistical uncertainty in the integrated cross sections [using an increment size of $d(\cos\theta) = 0.1$] plus the estimated one for the extrapolation. The total cross sections are smaller than 1 mb in the energy range 50–300 MeV, which constitutes coherent pion absorption as a rarity among reaction channels. We can illustrate this with the example $^4\text{He}(\pi^-, n)^3\text{He}$ at 150 MeV where (π^-, n) is 0.6 mb, which is less than 1% of the total pion absorption cross section (80 mb) and less than $\frac{1}{2}\%$ of the total reaction cross section (200 mb) (Ref. 24) or 5% of $\pi d \rightarrow pp$.²⁵ The decomposition of the

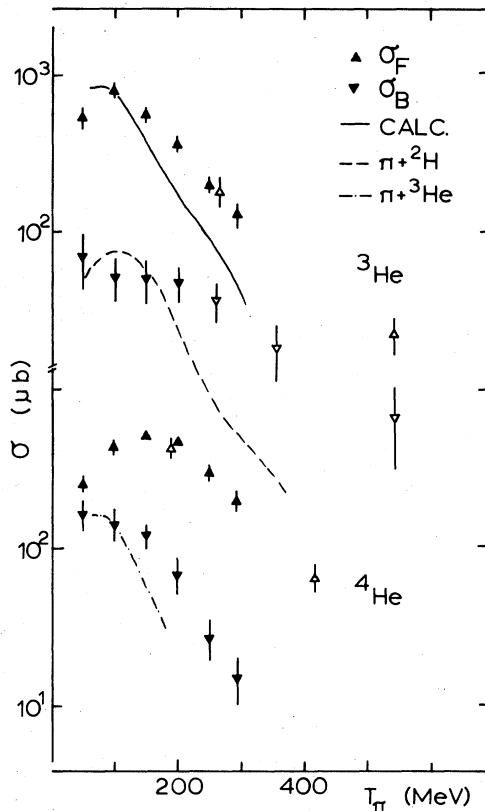


FIG. 11. The angle integrated cross section for the forward (σ_F) and backward (σ_B) hemispheres; (a) $^3\text{He}(\pi^-, n)^2\text{H}$ and (b) $^4\text{He}(\pi^-, n)^3\text{He}$; our results are complemented with previous data (Refs. 22 and 23) (solid and open symbols). The solid curve is the calculation of Ref. 10 and the broken lines represent $\sigma_B(\pi, \pi)$ for ^2H and ^3He deduced from Ref. 21.

(π^-, n) cross section into the partial angular integrated cross sections σ_F with $0 \leq \theta \leq 90^\circ$ and σ_B with $90^\circ < \theta \leq 180^\circ$ shows the forward angle dominance of these (π^-, n) reactions. It is most pronounced for $^3\text{He}(\pi^-, n)^2\text{H}$ at small energies and diminishes somewhat with increasing energy.

Alternatively, the measured differential cross section can be shown versus the reduced momentum transfer $q = |(1 - 1/A)\vec{p}_\pi - \vec{p}_n|$. We know that this is an important parameter because of the nuclear form factor involved in the dynamics of the (π, N) reaction, as is further discussed below. Our results on $(d\sigma/d\Omega)(q)$ for fixed incident energies are shown in Figs. 12 and 13. We find that there is a rapid decrease with q in the small angle region. Beyond 70° the falloff rate is much slower, which is particularly true for ^4He . If we search for features that show a pattern fixed in q , the forward angle slope is such a feature. It is also possible that the position of the break in the slope for $^3\text{He}(\pi^-, n)^2\text{H}$ is fixed in q and might tend to develop into a minimum at $q \approx 650 \text{ MeV}/c$ for $T_\pi > 200 \text{ MeV}$. Any similar q dependent features for $^4\text{He}(\pi^-, n)^3\text{He}$ would probably be masked by the strong θ dependence in the region $\theta > 70^\circ$.

Our data on $^3\text{He}(\pi^-, n)^2\text{H}$ at 100, 200, and 250 MeV overlap with previous measurements in the energy ranges 79–114,^{1,26,27} 162–176,^{27–29} and 256–266 MeV,^{27,29–32} and there is a previous experiment²² corresponding to our $^4\text{He}(\pi^-, n)^3\text{He}$ at 170 MeV. To utilize these results, most of which are for (p, π) reactions, we have expressed them as (π^-, n) cross sections using detailed balance and assuming isospin invariance so that $d\sigma(\pi^-, n) = d\sigma(\pi^+, p) = 2d\sigma(\pi^0, p)$. We find that for $^3\text{He}(\pi^-, n)^2\text{H}$ at 100 MeV, the results on the overall cross section magnitude seem to be consistent with the experimental uncertainties of some $\pm 20\%$, but there is some difficulty with the angular shape (Fig. 14). The back angle rise indicated in the data of Carrol *et al.*²⁷ are not in agreement with the present experiment nor with the experiment of Frank *et al.*¹ The (π, N) cross section does not vary much between 150 and 200 MeV so it is justified to use our 200 MeV angular distribution in comparison with the 160–180 MeV data. The agreement is very good between the four sets of data with two exceptions. At forward angles, the data of Crowe *et al.*²⁸ are a factor of 2 to 3 higher than ours. The other region of discrepancy is the extreme back angles where the sharp rise in the cross section as measured by Dollhopf *et al.*²⁹ is not confirmed by the present experiment. Other recent experiments³³

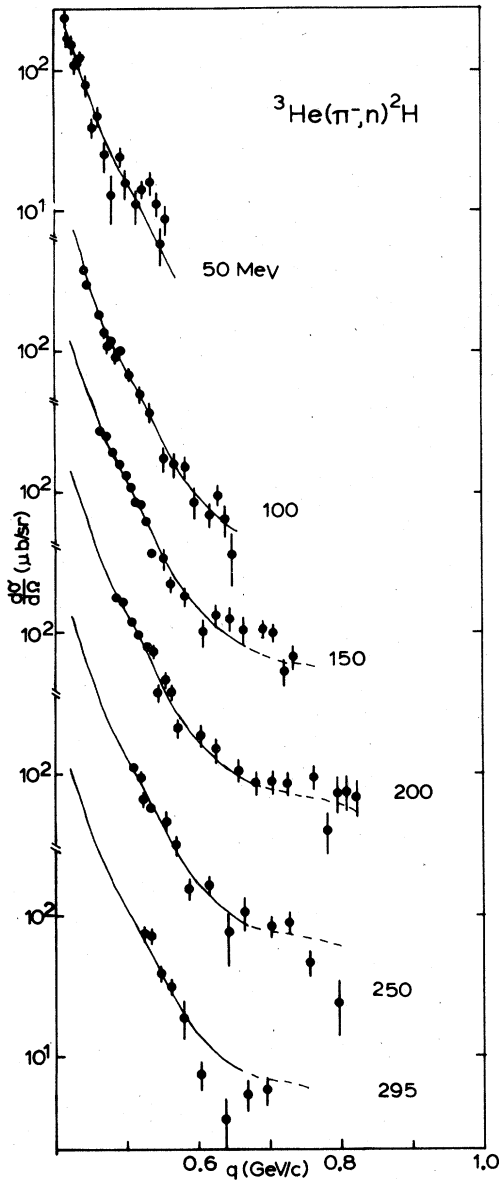


FIG. 12. The differential cross section of ${}^3\text{He}(\pi^-,n){}^2\text{H}$ at every 50 MeV between 50–295 MeV plotted versus the momentum transfer q . Also shown are the functions $G(q)$ that best fit the q dependence for forward angles (see the text).

have also not found a back angle rise. At 250 MeV there is good agreement between the measurements, except for the high point at $\theta = 97^\circ$ in the data of Aslanides *et al.*³² and our low point at $\theta = 104^\circ$. For ${}^4\text{He}(\pi^-,n){}^3\text{H}$ at 200 MeV the agreement is very good with the data of Tatischeff *et al.*²² corresponding to (π^+,p) at 176 MeV, although the second maximum is lower in the latter data.

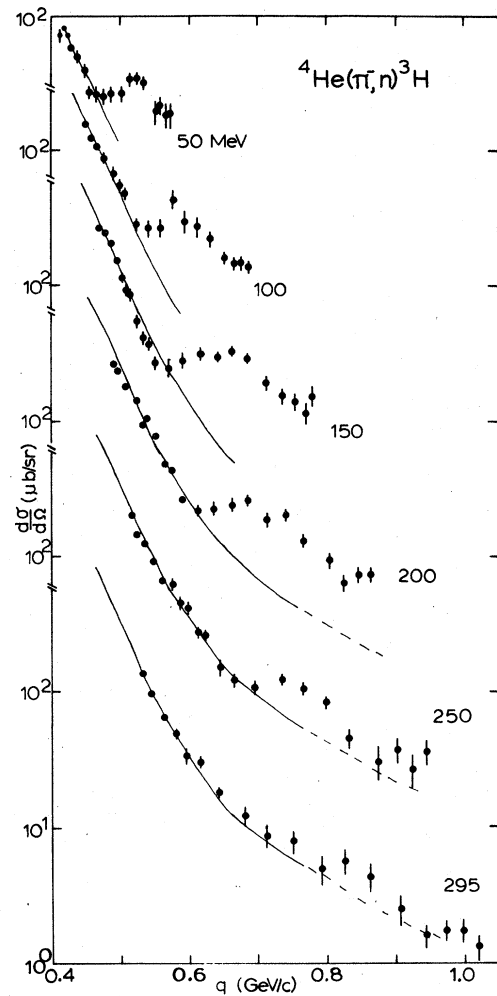


FIG. 13. The differential cross section of ${}^4\text{He}(\pi^-,n){}^3\text{H}$ at every 50 MeV between 50–295 MeV plotted versus the momentum transfer q . Also shown are the functions $G(q)$ that best fit the q dependence for forward angles (see the text).

IV. COMPARISON WITH CALCULATIONS

A. The two-nucleon pion absorption model

Most calculations performed on (π,N) in ${}^3,4\text{He}$ invoke explicitly multinucleon interactions for the basic pion absorption process of which we first consider the results of calculations based on two-nucleon interactions. The triangle diagram [Fig. 15(a)] has been used by Fearing¹⁰ to calculate (π,N) in ${}^3\text{He}$ and ${}^4\text{He}$. This (π,N) cross section is expressed principally in terms of the $\pi d \rightarrow pp$ cross section and an inelastic form factor^{10,34} $F^2(K)$, where K is related to q through

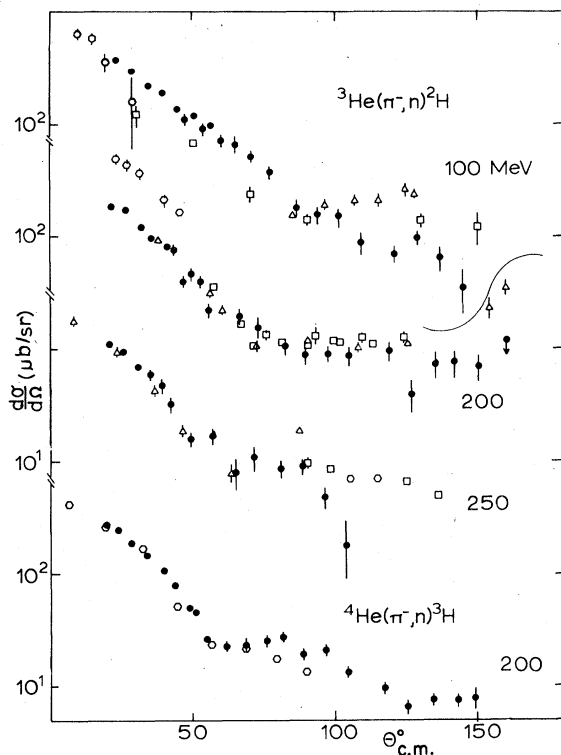


FIG. 14. Comparison of our results on ${}^3\text{He}(\pi, n){}^2\text{H}$ at 100, 200, and 250 MeV with other data at $T_\pi = 79-114$ (Refs. 1, 26, and 27), 162-176 (Refs. 27-29), and $T_\pi = 256-266$ (Refs. 27, 29-32), and our results on ${}^4\text{He}(\pi, n){}^3\text{H}$ at 200 MeV with other data at 170 MeV (Ref. 22).

$K = [(A-2)/(A-1)]q$. The underlying hypothesis is that the hard pion-nucleus interaction, constituting the elementary absorption process, is limited to a $\pi-2N$ interaction while other (soft) π -nucleus interactions that might take place are included as distortion effects. It is further assumed that the nuclear $2N$ state can be described as a quasi-deuteron, allowing the $\pi NN \rightarrow NN$ vertex to be represented by the $\pi d \rightarrow pp$ cross section. We have made use of Fearing's results which he obtained with correlated-Gaussian wave functions to describe the nuclear states with the deuteron d state included.

Other calculations are based on approximations for the $\pi-2N$ interactions that utilize the large probability for Δ formation in the $\pi+N$ scattering (isobar model) preceding the absorption step. We shall make use of the results from recent calculations of Green *et al.*⁵ to discuss some of the microscopic aspects of the $\pi-2N$ interaction in the

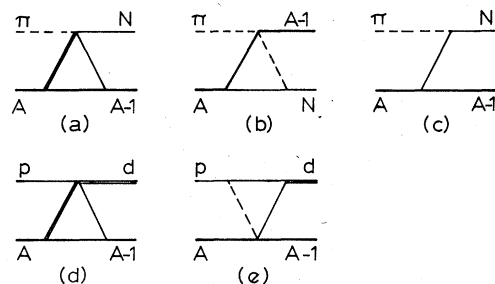


FIG. 15. Illustration of reaction processes discussed in the text: $A(\pi, N)A-1$ represented by (a) the two-nucleon pion absorption mechanism with $\pi d \rightarrow pp$ as subprocess; (b) the pion-core rescattering mechanism with $\pi + A-1$ elastic scattering as subprocess; (c) one-nucleon pion absorption. $A(p, d)A-1$ represented by (d) the two-nucleon interaction mechanism with $pd \rightarrow dp$ backscattering as subprocess; (e) pion-nucleon exchange with $A(\pi, N)A-1$ as sub process.

analysis of our data.

We start the discussion with ${}^3\text{He}(\pi^-, n){}^2\text{H}$, for which the most detailed calculations have been done. As can be seen in Fig. 16, the forward angle cross section is generally correctly predicted by Fearing and, for incident energies around the resonance, the agreement with the data is good over the whole angular range. (We disregard for the moment the need to renormalize the prediction to match the data.) One region this calculation misses is the large angles at the lowest energies where a back angle rise is predicted with a clear minimum around 90° that can be followed to higher energies. These features of the calculations might be a reflection of similar characteristics in the subprocess $\pi d \rightarrow pp$. Since the data do not show these systematics and they are not present in the isobar model prediction,⁵ it seems to be an artifact of the phenomenological representation of the pion interaction vertex. Otherwise, this model predicts very smooth angular distributions. Fearing observes that this is due to wave function antisymmetrization which prevents details in individual form factor contributions from showing up in (π^-, n) . This is not universally true for all two-nucleon models since the isobar model approach⁵ predicts a form factor produced minimum at $K \approx 360$ MeV/c. Experimentally, there is possibly a slight indication of a break in the (π^-, n) q dependence in this region (cf. Fig. 12), but if this were to be interpreted in terms of a form factor effect, it is much smaller than predicted by the isobar model.

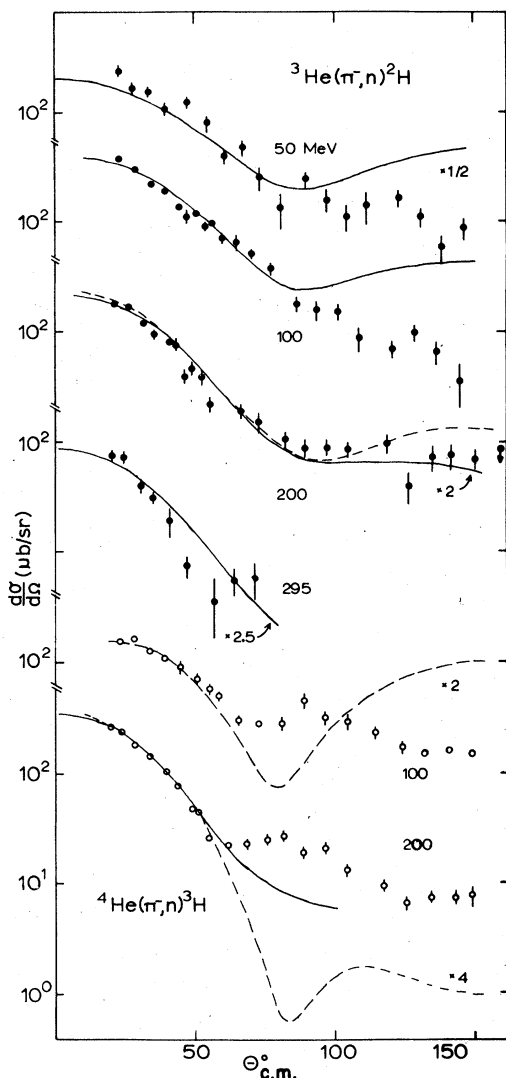


FIG. 16. Comparison of our angular distributions for ${}^3\text{He}(\pi^-,n){}^2\text{H}$ and ${}^4\text{He}(\pi^-,n){}^3\text{H}$ with calculated ones based on the quasideuteron absorption (solid lines) (Ref. 10) and the pion-core rescattering (dashed lines) (Refs. 20, 35, and 37) models.

The form factor as well as the distortion effects are important for the magnitude of the predicted cross sections. The latter effects are included by Fearing, which make his prediction match the data at around 100 MeV, but they also affect the functional form of the energy variation (Fig. 10). Without distortions, the general shape of the measured energy variation is better reproduced including the location of the maximum. The maximum is shifted down in energy relative to its position for

$\pi d \rightarrow pp$ (cf. Fig. 17) which can be attributed to the increasing form factor suppression with increasing K , and hence, T . The distortion, essentially the pion-nucleus attenuation, suppresses the cross section at resonance energies and causes a further downshift in energy of the predicted cross section, in disagreement with the data. In this regard, the incorporated distortion seems too strong and some of the needed magnitude reduction would have to be accounted for in some other way. The energy dependence is further discussed in Sec. V.

The ${}^4\text{He}(\pi^-,n)$ reaction is of particular interest because of the very clear angle dependent features in the cross section. The only $\pi - 2N$ calculation available is the one of Fearing which misses this feature of the data, i.e., the second maximum is not reproduced; the prediction at 200 MeV is shown in Fig. 16 (solid line) and compared with our data. Apart from this maximum, the ${}^3\text{He}(\pi,n){}^2\text{H}$ and ${}^4\text{He}(\pi,n){}^3\text{H}$ angular distributions (at $T = 200$ MeV) are very similar and are correctly predicted. The

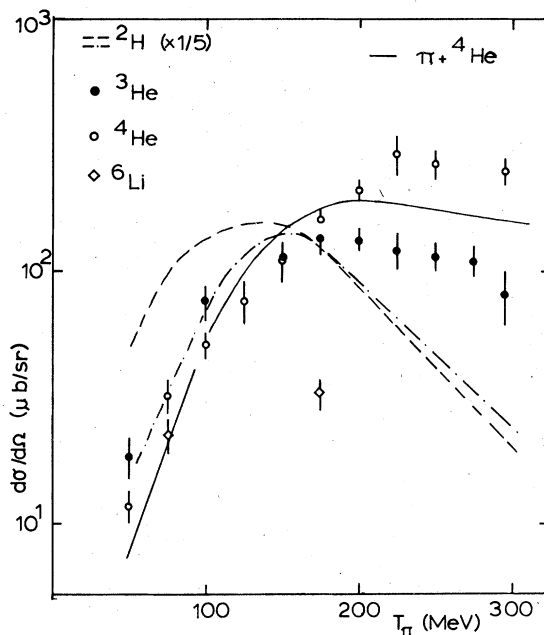


FIG. 17. Results of the energy dependence of ${}^3\text{He}(\pi^-,n){}^2\text{H}$ and ${}^4\text{He}(\pi^-,n){}^3\text{H}$ (solid and open dots) represented by the factor C compared with the differential cross sections (arbitrarily normalized) of $\pi + {}^4\text{He}$ elastic scattering (Ref. 40) at $\theta = 0^\circ$ (solid line) and of $\pi d \rightarrow pp$ (Refs. 2 and 25) at $\theta = 35^\circ$ and $\theta(Q_0)$ (dashed and dotted lines). Results are also shown for ${}^6\text{Li}(\pi^+,p){}^5\text{Li}$ (ground state transition) taken from Ref. 43.

two-nucleon pion interaction might, therefore, represent the general trend of the (π, n) reaction dynamics. The discrepancy for ${}^4\text{He}$, however, seems to indicate that the quasideuteron approximation does not take into account certain aspects of $\pi + N$ scattering in the absorption process which we shall discuss below.

B. The pion-core rescattering model

One way to account for the $\pi + N$ scattering part of the (π, n) is the pion-core rescattering model^{3,35,36} represented by the triangle diagram in Fig. 15(b). In contrast to the situation for the $\pi - 2N$ model, the number of $\pi + n$ interactions is not restricted to a single off-shell scattering as for the two-nucleon models (considered as $\pi + N_1 \rightarrow \pi + N_1$ followed by $\pi N_2 \rightarrow N_2$), but taken to be the same as what determines $\pi + A - 1$ elastic scattering. The fact that elastic scattering is mostly $\pi + N$ on-shell scattering constitutes a principal difference compared to the $\pi + N$ off-shell scattering which is likely to be involved in pion absorption. Gibbs *et al.*^{3,35} suggest an off-shell form factor $u^2[(1 - 1/A)\vec{p}_\pi - \vec{p}_p]$ to account for this difference. This factor together with the $\pi N \rightarrow N$ vertex function $f_{\pi NN}$ and a kinematic factor determine an overall scaling factor express $d\sigma/d\Omega(\theta_N)$ of $A(\pi, N)A - 1$ in terms of $d\sigma/d\Omega(\theta_\pi)$ of $A - 1(\pi, \pi)A - 1$ at a given pion energy.

This model predicts cross sections for ${}^3\text{He}(\pi^-, n){}^2\text{H}$ that are in fair agreement with our angular distributions at 200 MeV (Fig. 16). The results of the pion-core rescattering and quasideuteron calculations are quite similar (as to shape) for ${}^3\text{He}$ but differ significantly for ${}^4\text{He}$. The rescattering model predicts an angular dependence that is too strong in comparison with data at both 100 and 200 MeV; at 200 MeV the prediction is too low by an order of magnitude in the region $\theta \geq 70^\circ$. It seems, therefore, that the pion-nucleus dynamics of the (π, n) and (π, π) might not be the same.

One might argue that it is only when the momentum transfer is large in both (π, π) and (π, N) , i.e., at large angles, that one would expect the $\pi + N$ multiple scattering to be analogous in the two reactions. For this domain we find that the (π, n) cross section tends to fall off more slowly with increasing T than elastic scattering, as evidenced in the σ_B cross section show in Fig. 11. The rescattering model, however, would predict a nearly proportional behavior between (π, n) and (π, π) since the dominant part of the scaling factor, $u^2 f_{\pi NN}^2$, changes very little with

energy. This again indicates that there is a distinct dynamics related difference between $\pi + N$ scattering in elastic pion-nucleus scattering and pion absorption.

Still there are striking similarities in the angular distributions of pion absorption and elastic scattering which are most clearly seen for ${}^4\text{He}(\pi^-, n){}^3\text{H}$ and ${}^3\text{H}(\pi^-, \pi^-){}^3\text{H}$ [or ${}^3\text{He}(\pi^+, \pi^+){}^3\text{He}$] in the region $60^\circ - 100^\circ$ (Refs. 38 and 39). These elastic scatterings show a minimum at $\theta \approx 65^\circ$, as does $\pi + {}^4\text{He}$ (Refs. 38 and 40), which is believed to be a manifestation of elementary $\pi + N$ scattering.³⁷⁻⁴² For resonance dominance, the $\pi + N$ cross section has a minimum at $\theta = 90^\circ$ which is partly filled in by spin-flip contributions. For ${}^4\text{He}$, the spins of protons and neutrons are paired off, which blocks $\pi + N$ spin-flip contributions. This enhances the $\pi + N$ scattering minimum for $\pi + {}^4\text{He}$ and the shift in location (from 90° to 65°) is a kinematics effect due to the transformation from the $\pi + N$ to the $\pi + {}^4\text{He}$ c.m. frames. The similarity between $\pi^- + {}^3\text{H}$ (or $\pi^+ + {}^3\text{He}$) and $\pi + {}^4\text{He}$ in this respect is explained by the weakness of the $\pi^- + p$ (or $\pi^+ + n$) spin-flip amplitudes. Therefore, the observed similarity between ${}^4\text{He}(\pi^-, n){}^3\text{He}$ and $\pi + \text{He}$ elastic scattering does not necessarily imply that pion elastic scattering from the target or the core nucleus is part of (π, N) . Actually, any such phenomenological similarity may rather reflect nuclear structure imposed restrictions on the elementary $\pi + N$ scattering amplitudes common to (π, n) and (π, π) which can be further illustrated for the reaction ${}^3\text{He}(\pi^-, n){}^2\text{H}$.

The reaction ${}^3\text{He}(\pi^-, n){}^2\text{H}$ lacks the angle dependent features reminiscent of the $\pi + N$ elastic scattering amplitudes, as does $\pi + {}^2\text{H}$ elastic scattering. In general, the presence of the $\pi + N$ signature in $\pi + A$ reactions stems from a close connection between the π -nucleus and π -nucleon waves so that the same partial waves appear in both systems simultaneously. This is not necessarily true for $\pi + d$ scattering since the deuteron size is much larger than the $\pi - N$ range, allowing many $\pi + d$ partial waves to contribute even for $3,3$ dominance in the elementary $\pi + N$ amplitude. A quasideuteron in ${}^3\text{He}$, however, is bound to be smaller than the free deuteron so one might suspect that the rescattering model would suppress the $\pi + N$ signature in the predicted ${}^3\text{He}(\pi^-, N){}^2\text{H}$ cross section. On the other hand, scattering off the initial singlet 1S_0 pn state is not included in the rescattering model using the $\pi + d$ cross section. This is a source of the $\pi + N$ spin-flip amplitudes that would tend to fill in

the minimum. The neglect of such contributions would work in the opposite direction to the effects of not accounting for the quasideuteron size. Therefore, one should be cautious about conclusions based on the apparent similarity between the angular distributions of $\pi + {}^2\text{H}$ elastic scattering and ${}^3\text{He}(\pi^-,n){}^2\text{H}$. One would hope, however, that these special and different conditions for $\pi + N$ scattering in ${}^3\text{He}/{}^3\text{H}$ and ${}^4\text{He}$ could be utilized in quantitative calculations of ${}^{3,4}\text{He}(\pi,n){}^{2,3}\text{H}$ with a microscopic treatment of pion-core rescattering in order to illuminate the fundamental question of the elementary $\pi - N$ interaction in $\pi + A$ scattering and $A(\pi,N)A - 1$ absorption.

V. THE q AND T DEPENDENCES OF (π^-,n)

The identification of a true angular dependence in (π,n) points to the importance of hard (off-shell) $\pi + N$ scattering in the basic absorption process. Just as for the free $\pi + N$ scattering, one would expect the influence of the 3,3 resonance to be strong and contribute to the energy dependence of (π^-,n) . We consider this an intrinsic energy dependence of the reaction which is largely decoupled from the momentum transfer since $\pi + N$ does not vary much with q . The nuclear form factor is the part of the reaction dynamics that contains the principal momentum transfer dependence. A problem, however, is that there is no unique choice of variable to express this dependence.

For the one-nucleon reaction mechanism [see Fig. 15(c)], the effective momentum transfer q would be the appropriate variable, in which case the (π,n) cross section would be a function of the single particle wave function squared $[|\psi(q)|^2]$. It would also serve well for the nuclear form factor dependence $F^2(K)$ of the quasideuteron model of the $\pi - 2N$ mechanism where $K \approx q(A - 2)/(A - 1)$. For the $\pi - 2N$ mechanism in general, the momentum transfer is shared between a single particle wave function at the $A \rightarrow A - 1 + p$ vertex and a form factor [cf. Figs. 15(a) and 15(c)], resulting in a complicated nuclear structure dependence different from $F(K^2)$, which is also true for reaction mechanisms involving more than two nucleons. In all cases, it is the reduced momentum transfer q that has to be accommodated by the bound nuclear system. The multiplicity (m) of the πN interactions of each reaction mechanism allows the nuclear single particle dynamics to be sampled at $q' \approx q/m$, which determines the functional form of the q dependence. As

long as the pion energy (through, for instance, the strength of the $\pi + N$ interaction) does not discriminate between reaction mechanisms, the variable q would be useful when attempting to separate out the nuclear dynamics dependence of the (π^-,n) reaction in order to assess the intrinsic T dependence.

The most pronounced q dependence is observed for forward angles ($\theta < 70^\circ$) where the differential cross sections of (π^-,n) for both ${}^3\text{He}$ and ${}^4\text{He}$ falls off rapidly with increasing q (Figs. 12 and 13) and can be fairly well represented with the parametrization $d\sigma/d\Omega = C(T) \exp [(Q_0 - q)/\lambda]$. The q variation is expressed by the slope parameter λ and the off-set parameter Q_0 introduced as a matter of convenience ($Q_0 = 500$ MeV/c). The strong energy dependence appears in the factor C with some change in the value of λ as energy and target nucleus change. The variation in λ is small ($\lambda = 35 - 50$ MeV/c for ${}^3\text{He}$ and $45 - 55$ MeV/c for ${}^4\text{He}$), so a value of $\lambda_0 = 48$ MeV/c gives an average fair fit to the bulk of data for $\theta < 70^\circ$. The energy dependence of the (π^-,n) reaction is thus expressed by $C(T)$. As an alternative approach we determined the q dependence as the curve that best represented all data where the data $d\sigma/d\Omega(q)$ at each energy were adjusted in magnitude so as to optimize the overlap in the region $\theta < 70^\circ$. This was done for the reactions ${}^3\text{He}(\pi^-,n){}^2\text{H}$ and ${}^4\text{He}(\pi^-,n){}^3\text{H}$ separately and the result from this eyeball fitting procedure are the functions $g(q)$ arbitrarily normalized so that $g(q = Q_0) = 1$ for $Q_0 = 500$ MeV/c. To match the magnitude of $d\sigma/d\Omega(q)$ at each energy, and still considering only the region $\theta < 70^\circ$, we multiply by A which is our energy dependent scaling factor, i.e., $G(q) = A(T)g(q)$. This approach to analyze the ${}^{3,4}\text{He}(\pi^-,n){}^{2,3}\text{H}$ cross sections confirms the result of the energy dependence expressed by $C(T)$, while it indicates a slightly more complicated q dependence (see Figs. 12 and 13) than the exponential functional form, and possibly some difference between ${}^3\text{He}$ and ${}^4\text{He}$ might also be indicated.

A few interesting observations (Figs. 12 and 13) can be made about the (π^-,n) cross section relative to the q dependence expressed by $G(q)$. For ${}^3\text{He}$ the measured angular distributions stay very close to $G(q)$. Although there are obvious excursions for the larger angles, these are moderate compared to what is seen for ${}^4\text{He}(\pi^-,n){}^3\text{H}$. The ${}^4\text{He}(\pi^-,n){}^3\text{H}$ cross section at $\theta < 70^\circ$ is clearly above the $G(q)$ level which is true in particular for the lower energies. This might indicate that there are different

reaction mechanisms at play and their contributions depend on angle. Differences observed between ${}^3\text{He}$ and ${}^4\text{He}$ could in part be due to a stronger θ dependence for ${}^4\text{He}$ as mentioned above, and should not immediately be ascribed to nuclear dynamics differences between ${}^3\text{He}$ and ${}^4\text{He}$. It is difficult to unfold the θ dependence in the cross section and its residual effect on the extracted momentum transfer dependence. Below we shall estimate its possible impact on the deduced energy dependence by comparing $C(T)$ of the exponential parametrizations of the (π, n) cross section with the $\pi d \rightarrow pp$ cross section.

Because of the weak q dependence of $\pi d \rightarrow pp$, the cross section at fixed angle (say at $\theta = 35^\circ$) represents the energy dependence of this reaction.²⁵ The angular variation, at fixed energy, is about a factor of 4 between 0° and 90° . By virtue of the normalization procedure used, $C(T)$ refers to the (π^-, n) cross section at $\theta = 35^\circ$ (the center of the region $\theta < 70^\circ$ fitted) but in order to separate out the q dependence, it is always expressed at $q = Q_0 = 500 \text{ MeV}/c$ using the q dependence of the exponential parametrization in terms of angles; this means an extrapolation from $\theta = 35^\circ$ to 90° at 50 MeV and from $\theta = 35^\circ$ to 0° at 280 MeV. We might, therefore, use the difference in $\pi d \rightarrow pp$ cross section at $\theta = 35^\circ$ and θ ($Q_0 = 500 \text{ MeV}/c$) as a measure of the uncertainty in using $C(T)$ to represent the intrinsic energy dependence of (π^-, n) in ${}^{3,4}\text{He}$. We can see from Fig. 17 that the residual θ dependence might suppress $C(T)$ for the lowest energies.

The results on the energy dependence are shown in Fig. 17. Characteristic for the (π^-, n) reactions in both ${}^3\text{He}$ and ${}^4\text{He}$ is a sharp rise in $C(T)$ with increasing energy reaching a pronounced maximum between 200 and 250 MeV. The energy dependence of ${}^{3,4}\text{He}(\pi^-, n)^{2,3}\text{H}$ resembles that of $\pi^- + n$ or $\pi + \text{He}$ elastic scattering which is largely dictated by the $\pi + N$ 3,3 resonance. In comparison, the $\pi d \rightarrow pp$ reaction has a maximum below resonance energy ($T \approx 150 \text{ MeV}$) and it shows a slower rate of increase up to the maximum and a faster decline above the maximum. The $\pi d \rightarrow pp$ reaction is also greatly affected by the resonance but calculations have shown how its influence is damped and moderated by pion exchange πN form factors⁸ or more general meson exchange effects.⁶ Those effects have not yet been theoretically assessed for (π, n) in ${}^{3,4}\text{He}$. Aside from the possible residual θ effect on $C(T)$ there are very clear differences between $\pi d \rightarrow pp$ and (π^-, n) in ${}^{3,4}\text{He}$ which can be commented upon in view of the following differ-

ences between ${}^2\text{H}$ and ${}^3\text{He}/{}^4\text{He}$. First, the average nucleon separation might be an important parameter and in this regard the deuteron is an odd species among the nuclei with an exceptionally small nucleon density. Yet, recent measurements¹ of pion absorption on quasifree NN pairs in ${}^{3,4}\text{He}$ have shown that the difference between the energy dependence of $\pi NN \rightarrow Np$ in ${}^{3,4}\text{He}$ and $\pi d \rightarrow pp$ is small, of the order of 60%. Second, the bound nuclear final state of ${}^{3,4}\text{He}(\pi^-, n)^{2,3}\text{H}$ marks a difference to $\pi d \rightarrow pp$, not only as to the q -dependent nuclear form factor involved [which is hopefully unfolded from $C(T)$], but it also implies that the pion interacts with nucleons that are not on the mass shell. Within the framework of the quasideuteron model (Fig. 15) the maximum is predicted to occur at $T_\pi \approx 163$ or 263 MeV depending on whether the quasideuteron or the nucleon is off the mass shell.⁹ Experimentally, it is observed between those extremes at $T_\pi \approx 200 \text{ MeV}$. Because of the inevitable ambiguities in the prescriptions for kinematics transformations^{9,10} involved, this should be considered an illustration of the shift in the location of the resonance in coherent pion absorption in nuclei due to off-mass shell effects.

VI. THE NUCLEAR STATE DEPENDENCE

The (π^-, n) reaction in ${}^{3,4}\text{He}$ involves pion interaction with nucleons principally in the $1s$ configuration. For target nuclei with $A > 4$ other configurations are likely to contribute as (π^+, p) on ${}^{6,7}\text{Li}$ going to the first few states in the residual nuclei ${}^{5,6}\text{Li}$ via predominant pion interactions with nucleons in the $1p$ configuration. Besides the difference in the kind of configurations contributing to (π, N) , there is also a considerable size difference between ${}^{3,4}\text{He}$ and ${}^{6,7}\text{Li}$ to remember. Despite the mentioned nuclear structure differences, (π, N) cross sections for He and Li are very similar,⁴³ and have nearly exponential q dependence in the angular region $\theta < 70^\circ$. The energy dependence, however, is not the same for these (π, N) reactions and to some extent there is a difference between the isotopes ${}^3\text{He}/{}^4\text{He}$ or ${}^6\text{Li}/{}^7\text{Li}$ just as there is between the two final states of ${}^7\text{Li}(\pi, p){}^6\text{Li}$. It is not clear what makes the q dependence not reflect the obvious changes in the nuclear structure considering that it seems to affect the energy dependence.⁴³ The fact, however, that the (π^+, p) data⁴³ at $T_\pi = 75$ and 175 MeV exhibit no signature of the $\pi + N$ minimum seen in ${}^4\text{He}(\pi^-, n){}^3\text{H}$ could be attributed to the size of Li and the subsequent mixing of $\pi + N$ partial waves discussed above.

VII. COMPARISON BETWEEN (π, N) AND (p, d) IN ${}^4\text{He}$

The (p, d) reaction is akin to (π, N) as a single nucleon transfer process although the projectile-nucleon interaction is much weaker and lacks the resonances of the $\pi + N$ system. The achievable momentum transfers are large for both reactions and with the now available data for ${}^4\text{He}$, from the present experiment and Ref. 44, we can compare the q dependences up to about 0.8 GeV/c. The average falloff of ${}^4\text{He}(p, d){}^3\text{He}$ and ${}^4\text{He}(\pi^-, n){}^3\text{H}$ with q is conspicuously similar, as can be seen in Fig. 18. This strongly suggests that the nuclear dynamics enter the reactions in similar ways to produce the large momentum transfer. The difference in $\pi + N$ and $p + N$ interaction strength seems not to affect the reaction mechanism. We also observe that the absence of the energy dependence in the

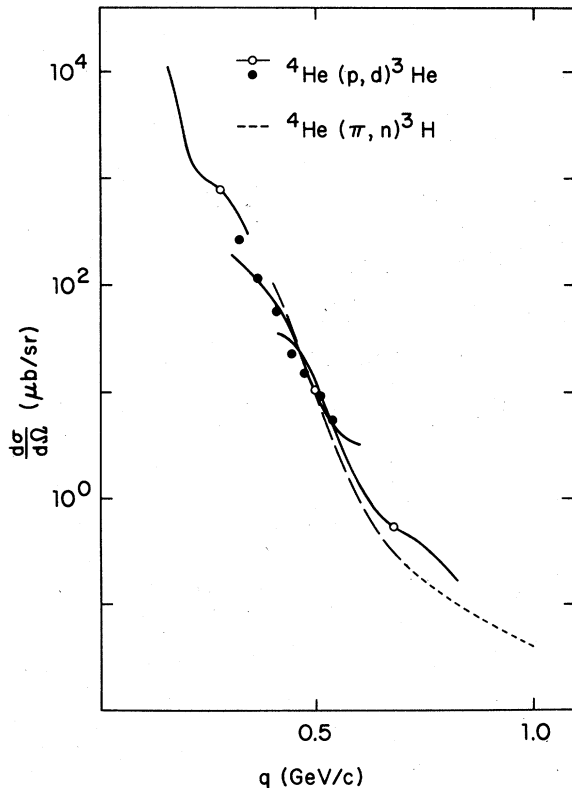


FIG. 18. The experimental angular distributions of ${}^4\text{He}(p, d){}^3\text{He}$ at 155, 435, and 770 MeV (represented by smooth curves) and data at $\theta_l = 22.5^\circ$ and $T = 200 - 500$ MeV (solid circles) (Ref. 44). The dashed line is the momentum dependence of ${}^4\text{He}(\pi^-, n){}^3\text{H}$ discussed in the text (arbitrarily normalized).

$p + N$ interaction is consistent with the lack of any strong energy dependence in (p, d) so that q is almost a perfect scaling variable for the (p, d) cross section.⁴⁵

Just as for the (π, N) reaction, one can prescribe⁴⁴⁻⁴⁶ a two-nucleon reaction model for (p, d) . It can be approximated with triangle graphs for (π, N) and (p, d) using the subprocesses $\pi d \rightarrow pp$ and $pd \rightarrow dp$, respectively (Fig. 15). The subprocess contains the reaction energy dependence and the nuclear form factor expresses the q dependence. The same form factor appears for both reactions and warrants the similarity in q dependence observed for (π, N) and (p, d) . The subprocesses ($\pi d \rightarrow pp$ and $pd \rightarrow dp$ back scattering) give the qualitative difference in energy dependence between the two processes.

Another approach has been suggested to describe the $A(p, d)A - 1$ reaction with a triangle diagram with $A(\pi, N)A - 1$ as a subprocess.⁴⁷ Without specifying a microscopic reaction mechanism for either reaction, it gives a formal justification for an inclusive comparison of (p, d) and (π, N) and prescribes how to perform the kinematics transformations. This scheme also indicates the qualitative similarity in the reaction dynamics of (π, N) and (p, d) , but it is first above $T_\pi \approx 100$ MeV or $T_p \approx 300$ MeV that the pionic contributions to (p, d) would be dominant and it would come on very strongly, as suggested by the (π, N) energy dependence. The data,⁴⁴ however, indicate no basic change in q dependence at this energy so the relationship between $A(p, d)A - 1$ and $A(\pi, N)A - 1$ is more intricate than that between, for instance, $p + A$ backscattering and $A(\pi, p)A - 1$ for reasons discussed in Ref. 45. On the contrary, the ${}^4\text{He}(p, d){}^3\text{He}$ reaction, as do other (p, d) reactions, shows a very smooth dependence on q over an extended range of q ($\sim 100 - 800$ MeV/c) with no obvious discontinuities. Actually, it is surprising that the momentum transfer region $q < 300$ MeV/c, which we believe to be dominated by single nucleon pickup, continues smoothly into the region $q > 300$ MeV/c where multinucleon reaction mechanisms are likely to contribute. This indicates to us that multinucleon contributions set in when the single particle amplitude $|\psi(q)|^2$ suppression of the one-nucleon contribution becomes critical. It will be controlled by q to the extent that the energy dependence of the multinucleon mechanism is of subordinate importance. The similarities in q dependence between (p, d) and (π, N) , starting already at $T_\pi = 50$ MeV or $T_p = 230$ MeV, point to a simi-

larity in multinucleon reaction mechanisms rather than a direct relationship between the cross sections. Since we have strong reasons to believe that the one-nucleon interaction is a negligible contributor to (π, N) , the same would be true for (p, d) at say $q > 300$ MeV/c. As more data on ${}^4\text{He}(p, d){}^3\text{He}$ become available, it would be of interest to see whether an indication of change in q dependence could be found.

VIII. SUMMARY

Comprehensive data for the (π^-, n) reactions in ${}^3,4\text{He}$ have been presented covering the kinematics regions $T = 50 - 300$ MeV, $\theta \approx 20^\circ - 150^\circ$, and $q \approx 0.4 - 1.0$ GeV/c. The phenomenological analysis of the data indicates both in the θ and T variables compelling evidence of $\pi + N$ (off-shell) scattering in the primary absorption process. Most conspicuous is the θ dependence of ${}^4\text{He}(\pi^-, n){}^3\text{H}$ which mirrors characteristic features of $\pi + \text{He}$ elastic scattering. The nuclear form factor q dependence is most evident for forward angles ($\theta < 70^\circ$). It shows little correlation with T , indicating that the reaction mechanism is not changing with energy and, hence, also not with the strength of the πN interaction. It is observed that since the (p, d) reaction, determined by the much weaker pN interaction, shows a q dependence very similar to (π^-, n) , it is the momentum transfer rather than the projectile/ejectile-nucleon interaction that determines the reaction mechanism. This would be true for forward angles. The large angle region of the (π^-, n) cross sections is not simple to factorize in

terms of θ , T , and q and one might suspect that other reaction mechanisms are at play here. From comparisons with predictions based on the pion-core rescattering model we find that the $\pi + N$ on-shell scattering dominating the π -nucleus dynamics of elastic scattering is not representative of the $\pi + N$ off-shell scattering believed to be part of the (π, N) absorption process. Calculations based on hard pion interactions with two nucleons are found to have some success in reproducing the gross features of the (π, N) reaction dynamics. The most specific predictions originate from invoking the $\pi d \rightarrow pp$ cross section for the $\pi - 2N$ interaction. This approximation, however, leaves an angular dependence feature characteristic of $\pi d \rightarrow pp$ that is foreign to the ${}^3,4\text{He}(\pi^-, n){}^2,3\text{H}$ angular distributions, while it fails to reproduce the detailed angular dependence of ${}^4\text{He}(\pi^-, n){}^3\text{H}$ reminiscent of the $\pi + N$ scattering amplitude. The partial success of this approach should encourage new theoretical attempts along the line of microscopic treatment of the $\pi - 2N$ interaction in order to unravel the physics behind the phenomenological features of apparent $\pi + N$ (off-shell) scattering recorded in this experiment.

ACKNOWLEDGMENTS

We are indebted to G. R. Burleson, J. S. McCarthy, C. F. Moore, and H. A. Thiessen for their support and we acknowledge the valuable contributions to the experiment by C. A. Goulding, C. L. Morris, and R. R. Whitney. This experiment was supported by the U. S. Department of Energy and the A. Welsh Foundation.

*Present address: SIN, Villigen, Switzerland.

†Present address: Eidg. Technische Hochschule, Zurich.
W. H. B. Chan Co., Los Angeles, California.

¹W. J. Frank, R. C. Bandtel, R. Madey, and B. J. Moyer, Phys. Rev. **94**, 1716 (1954).

²D. F. Measday and G. A. Miller, Annu. Rev. Nucl. Part. Sci. **29**, 121 (1979); B. Hoistad, Adv. Nucl. Phys. **11**, 135 (1979).

³W. R. Gibbs, in *Proceedings of the Conference on Nucleon-Nucleon Interactions, Vancouver, Canada, 1977*, edited by D. F. Measday, H. W. Fearing, and A. W. Strathdee (AIP, New York, 1978), p. 314.

⁴M. Dillig and M. G. Huber, Lett. Nuovo Cimento. **16**, 293 (1976).

⁵A. M. Green and M. E. Sainio, Nucl. Phys. **A232**, 349 (1980).

⁶J. Chai and D. O. Riska, Nucl. Phys. **A338**, 349 (1980).

⁷J. A. Niskanen, Nucl. Phys. **A298**, 417 (1978); Phys. Lett. **82B**, 187 (1979).

⁸B. Goplen, W. R. Gibbs, and E. L. Lomon, Phys. Rev. Lett. **32**, 1012 (1974).

⁹G. W. Barry, Phys. Rev. **D 7**, 1441 (1973).

¹⁰H. W. Fearing, Phys. Rev. **C 16**, 313 (1977); J. H. Alexander and H. W. Fearing, in *Meson-Nuclear Physics—1976 (Carnegie-Mellon Conference)*, Proceedings of the International Topical Conference on Meson-Nuclear Physics, edited by P. D. Barnes, R. A. Eisenstein, and L. S. Kisslinger (American Institute of Physics, New York, 1976), p. 468; H. W. Fearing (private communication).

¹¹J. Källne *et al.*, Phys. Lett. **97B**, 205 (1980).

- ¹²R. R. Whitney, thesis, Stanford University, 1971; J. S. McCarthy, I. Sick, and R. R. Whitney, Phys. Rev. C **15**, 1396 (1977).
- ¹³J. E. Bolger, H. Ellinger, and C. F. Moore, Comp. Phys. Commun. **16**, 345 (1979); J. E. Bolger, thesis, University of Texas at Austin, 1977 (unpublished).
- ¹⁴H. A. Thiessen *et al.*, Los Alamos Scientific Laboratory Report LA-6663-MS, 1976 (unpublished); R. Boudrie (private communication).
- ¹⁵P. J. Bussey *et al.*, Nucl. Phys. **B58**, 363 (1973).
- ¹⁶K. M. Crowe, A. Fainberg, J. Miller, and A. S. L. Parsons, Phys. Rev. **180**, 1349 (1969).
- ¹⁷J. Källne, A. Obst, and H. A. Thiessen, Los Alamos Scientific Laboratory LA-6356-MS, 1976 (unpublished).
- ¹⁸D. F. Measday and C. Richard-Serre, Nucl. Instrum. Methods **76**, 45 (1969).
- ¹⁹N. Willis, I. Brissaud, L. Bimbot, Y. LoBornec, and B. Tatischeff, Nucl. Phys. **A233**, 121 (1974).
- ²⁰J. Källne *et al.*, Phys. Rev. Lett. **40**, 378 (1978).
- ²¹J. H. Norem, Nucl. Phys. **B33**, 512 (1971); K. Gabathuler *et al.*, *ibid.* **B55**, 397 (1973); D. Axen *et al.*, *ibid.* **A256**, 387 (1976); D. D. Brayshaw and E. Ferreira, Phys. Lett. **68B**, 139 (1977); R. H. Cole *et al.*, Phys. Rev. C **17**, 181 (1978).
- ²²B. Tatischeff *et al.*, Phys. Lett. **63B**, 158 (1976).
- ²³J. Banaigs *et al.*, Phys. Lett. **45B**, 363 (1978).
- ²⁴M. Hirata and F. Lenz, Ann. Phys. (N.Y.) **108**, 116 (1977).
- ²⁵C. Richard-Serre *et al.*, Nucl. Phys. **B20**, 413 (1970).
- ²⁶K. R. Chapman *et al.*, Nucl. Phys. **57**, 499 (1964).
- ²⁷J. Carrol *et al.*, Nucl. Phys. **A305**, 502 (1978).
- ²⁸A. V. Crowe, B. Ladley, E. Lillethun, S. M. Mascowitz, and C. Rey, Phys. Rev. **118**, 1091 (1960).
- ²⁹W. Dollhopf *et al.*, Nucl. Phys. **A217**, 381 (1973).
- ³⁰N. E. Booth, Phys. Rev. **132**, 2305 (1963).
- ³¹D. Hartig *et al.*, Phys. Rev. **119**, 1716 (1960).
- ³²E. Aslanides *et al.*, Phys. Rev. Lett. **39**, 1654 (1977).
- ³³J. Franz *et al.*, Phys. Lett. **93B**, 384 (1980).
- ³⁴M. R. Locher and H. J. Weber, Nucl. Phys. **B76**, 400 (1974).
- ³⁵W. R. Gibbs and A. T. Hess, Phys. Lett. **68B**, 205 (1977).
- ³⁶U. S. Bhasin, Phys. Lett. **69B**, 297 (1977).
- ³⁷R. H. Landau, Phys. Rev. C **15**, 2127 (1977).
- ³⁸J. Källne *et al.*, Phys. Rev. Lett. **45**, 517 (1980).
- ³⁹Yu A. Scherbakov *et al.*, Nuovo Cimento **31A**, 262 (1976).
- ⁴⁰F. Binon *et al.*, Nucl. Phys. **A289**, 499 (1978).
- ⁴¹B. Nefkens, *Lecture Notes in Physics* (Springer, Berlin, 1978), Vol. 87, p. 189.
- ⁴²J. Källne *et al.*, Phys. Rev. Lett. **103B**, 13 (1981).
- ⁴³J. Källne *et al.*, Phys. Rev. C **21**, 2681 (1980).
- ⁴⁴J. Källne *et al.*, Phys. Rev. Lett. **41**, 1638 (1978).
- ⁴⁵J. Källne and P. C. Gugelot, Phys. Rev. C **20**, 1085 (1979).
- ⁴⁶J. Källne *et al.*, Phys. Rev. C **21**, 675 (1980).
- ⁴⁷C. Wilkin, J. Phys. G **6**, 69 (1980).